High-order TENO scheme for high-speed flows

By L. Fu† AND K. P. Griffin

1. Motivation and objectives

In the future, very-high-Mach-number vehicles flying at low altitudes could play an important role in global transportation (Urzay 2018). By flying at relatively low altitudes, these systems can use ambient atmospheric oxygen for combustion, instead of conventional rockets, which carry their oxidizer in cryogenic tanks, the weight of which substantially reduces the efficiency of such transportation systems. While the thicker atmosphere is good for air-breathing propulsion, it leads to immense aerodynamic heating, which necessitates accurate numerical simulation to design safe and reliable systems. High-speed flows are numerically challenging to simulate due to the formation of shock waves, which are discontinuities in the continuous governing equations (Shu 2009; Pirozzoli 2011; Fu *et al.* 2021; Griffin *et al.* 2021), which are governed by hyperbolic conservation laws. In turbulent flows, it is also essential that the methods have very low numerical dissipation as not to artificially suppress turbulence. In addition, numerical robustness, which is the property that the solution remains bounded (does not blow up), is essential.

Since the 1980s, many numerical approaches have been developed, such as the artificial viscosity scheme (Von & Richtmyer 1950; Jameson 1994), total variation diminishing scheme (Harten 1983), essentially non-oscillatory (ENO) (Harten *et al.* 1987) scheme and weighted essentially non-oscillatory (WENO) scheme (Liu *et al.* 1994). Among these approaches, the WENO scheme has been widely used in both academic and engineering simulations due to the sharp and robust shock-capturing capabilities. However, there are still some drawbacks, e.g., the order-degeneration near critical points, generating excessive numerical dissipation for small-scale structures, and the lack of numerical robustness for very-high-order reconstructions. Improvements for the order degeneration problem include the WENO-M scheme (Henrick *et al.* 2005) and the WENO-Z scheme (Borges *et al.* 2008). The numerical dissipation can be reduced by increasing the order of accuracy (Gerolymos *et al.* 2009), switching between a low-dissipation and a shock-capturing scheme based on a shock senor (the hybrid concept) (Adams & Shariff 1996), and optimizing the spectral properties of the scheme (improving the modified wavenumber) (Lele 1992; Weirs & Candler 1997). For enhancing the robustness of the scheme, Suresh & Huynhb (1997) propose to bound the solution near discontinuities by a monotonicity-preserving limiter. The order-reduction approach (Gerolymos *et al.* 2009; Titarev & Toro 2004), which recursively resorts to lower-order stencils, is an alternative way to improve the robustness of WENO schemes.

However, when the above mentioned numerical approaches are applied to very-high-Mach-number flows with vacuum or near-vacuum regions, e.g., for applications with low density and low pressure, numerical difficulties may occur due to the presence of negative density and pressure. Although these high-order shock-capturing schemes generate entropy solutions for hyperbolic conservation laws (i.e., entropy monotonically increases), in general, they may fail to preserve positivity, which eventually causes the numerical

† Currently at Hong Kong University of Science and Technology

solution to become unbounded. In a series of works, Zhang & Shu (2010, 2012) successfully develop a positivity-preserving limiter for numerical methods in discontinuous Galerkin, finite-difference, and finite-volume frameworks. Extensive validations reveal that the high-order accuracy is preserved asymptotically and the positivity of density and pressure is maintained with a certain Courant-Friedrichs-Lewy (CFL) constraint when a strong-stability-preserving (SSP) Runge-Kutta method is employed for the temporal integral.

Recently, Fu *et al.* (2016, 2017) have proposed a family of high-order targeted ENO (TENO) schemes for hyperbolic conservation laws. The performance has been demonstrated for complex fluid simulations, e.g., multiphase flows (Haimovich & Frankel 2017), detonation simulations (Dong *et al.* 2018), a hypersonic boundary layer with finite rate chemistry (Di Renzo *et al.* 2020; Di Renzo & Urzay 2021), curvilinear geometry (Fu 2018), finite-volume gas dynamics simulations (Sun *et al.* 2016; Fu 2018) and turbulent flows (Fu *et al.* 2018*b*). In a work by Fu *et al.* (2018*a*), the TENO weighting strategy is proposed to function as an explicit shock detector, which enables the design of an interpolation scheme with optimal order even near the discontinuities, and an adaptive dissipation control strategy is invented for further reducing the numerical dissipation. In this paper, by incorporating a simple and effective positivity-preserving limiter, the eight-point TENO8-NA scheme (Fu *et al.* 2018*a*) is extended to very-high-Mach-number flows, and the performance in terms of preserving the low numerical dissipation and ENO property is addressed by computing challenging benchmark simulations.

The remainder of this paper is organized as follows: in Section 2, the construction of the high-order TENO-NA scheme is briefly reviewed. In Section 3, the positivity-preserving limiter is introduced for the Euler equations. In Section 4, a set of benchmark cases is simulated to demonstrate the performance of the presented scheme. Concluding remarks and future work will be discussed in Section 5.

2. Construction of high-order TENO-NA schemes

We consider the one-dimensional hyperbolic conservation law

$$\frac{\partial u}{\partial t} + \frac{\partial}{\partial x} f(u) = 0, \tag{2.1}$$

where x denotes the spatial coordinate, t denotes the time coordinate, u denotes the solution, and f is the flux function $\partial f(u)/\partial u > 0$. Eq. (2.1) can be spatially discretized in a conservative form following

$$\frac{du_i}{dt} \approx -\frac{1}{\Delta x}(\widehat{f}_{i+1/2} - \widehat{f}_{i-1/2}), \tag{2.2}$$

where Δx is the grid spacing and the numerical flux $\hat{f}_{i\pm1/2}$ is computed from a convex combination of $K-2$ candidate-stencil fluxes

$$\widehat{f}_{i+1/2} = \sum_{k=0}^{K-3} w_k \widehat{f}_{k,i+1/2}, \tag{2.3}$$

with K-point reconstruction. To obtain a Kth-order approximation for $\widehat{f}_{i+1/2}$, a (r_k-1)-degree interpolation on each candidate stencil leads to

$$\hat{f}_k(x) = \sum_{l=0}^{r_k-1} a_{l,k} x^l, \tag{2.4}$$

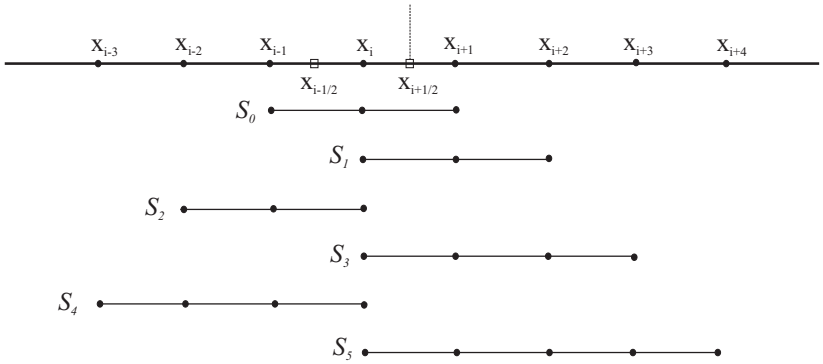

FIGURE 1. Candidate stencils with incremental widths. Assuming that the information signal propagates from the left to the right with $\partial f(u)/\partial u > 0$, each candidate stencil contains at least one point upwind with respect to the data reconstruction at cell interface $i + 1/2$. The reconstruction scheme for the scenario $\partial f(u)/\partial u < 0$ can be obtained by mirroring the stencils about $x_{i+1/2}$.

where r_k denotes the stencil width of candidate flux $\hat{f}_k(x)$.

2.1. *Candidate stencils with incremental widths*

TENO schemes combine stencils of incremental widths as shown in Figure 1. The advantages are that (1) both odd and even order schemes can be constructed in a unified framework and that (2) the numerical robustness of the WENO5-JS scheme is preserved even for very-high-order reconstruction, as the smallest three candidate stencils are the same.

2.2. *Scale separation*

Scale separation of discontinuities from smooth waves is achieved by defining the unnormalized smoothness indicator

$$\gamma_k = \left(C + \frac{\tau_K}{\beta_{k,r_k} + \varepsilon} \right)^q, \ k = 0, \cdots, K-3, \tag{2.5}$$

where $\varepsilon = 10^{-40}$, $q = 6$ and $C = 1$. Following Jiang & Shu (1996), β_{k,r_k} can be computed as

$$\beta_{k,r_k} = \sum_{j=1}^{r_k-1} \Delta x^{2j-1} \int_{x_{i-1/2}}^{x_{i+1/2}} \left[\frac{d^j}{dx^j} \hat{f}_k(x) \right]^2 dx. \tag{2.6}$$

τ_K is defined as (Fu *et al.* 2017)

$$\tau_K = \beta_K - \frac{1}{6}(\beta_{1,3} + \beta_{2,3} + 4\beta_{0,3}) = O(\Delta x^6), \tag{2.7}$$

where β_K measures the global smoothness on the K-point full stencil.

2.3. *ENO-like stencil selection and adaptive dissipation control*

The smoothness indicator is normalized as (Fu *et al.* 2016)

$$\chi_k = \frac{\gamma_k}{\sum_{k=0}^{K-3} \gamma_k}, \tag{2.8}$$

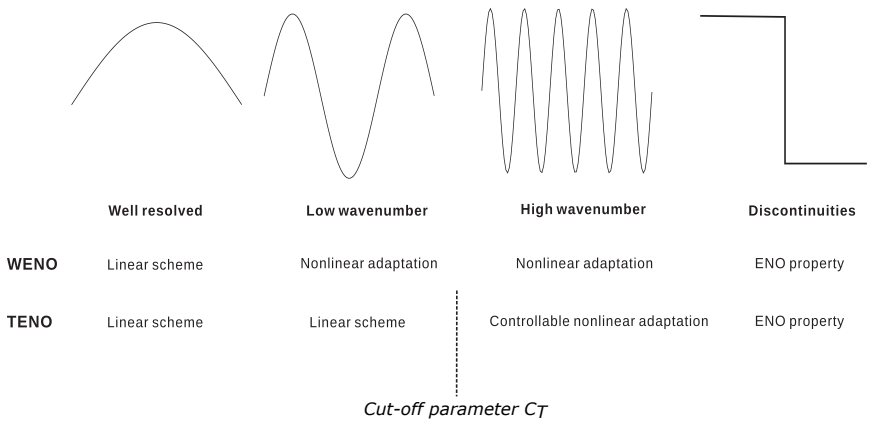

FIGURE 2. Resolution comparisons between WENO and TENO schemes (without adaptive dissipation control) for well-resolved scales, low-wavenumber scales, high-wavenumber scales and discontinuities.

and then filtered by a sharp cutoff function

$$\delta_k = \begin{cases} 0, & \text{if } \chi_k < C_T, \\ 1, & \text{otherwise}, \end{cases} \tag{2.9}$$

where the non-dimensional parameter C_T determines whether or not a stencil is identified as "smooth."

With this new ENO-type stencil selection strategy, the spectral properties of the underlying linear scheme can be recovered exactly up to intermediate wavenumbers and the accuracy order of the underlying linear scheme is preserved without degenerations (Fu *et al.* 2016, 2017). The performance difference between the classical WENO scheme and the TENO scheme for resolving a wide range of scales is given in Figure 2.

However, further analysis reveals that the above weighting strategy fails to distinguish the high-wavenumber fluctuations from genuine discontinuities. Consequently, excessive numerical dissipation is generated for high-wavenumber fluctuations and the small-scale structures are smeared significantly. In Fu *et al.* (2018*b*,*a*), an adaptive dissipation control strategy is proposed to improve the performance for high-wavenumber fluctuations.

The upper and lower bounds of C_T in Eq. (2.9) are determined by numerical experiments and spectral analyses. The new adaptation strategy for C_T is defined as

$$\begin{cases} g(m) = (1-m)^4(1+4m), \\ \beta = \alpha_1 - \alpha_2\left[1 - g(m)\right], \\ C_T = 10^{-\lfloor \beta \rfloor}, \end{cases} \tag{2.10}$$

where $\lfloor \beta \rfloor$ denotes the floor function (Gauss bracket) of β, $g(m)$ is a smoothing-kernel-based mapping function, the constant parameters are $\alpha_1 = 10.5$ and $\alpha_2 = 3.5$. When $m \approx 1$, $g(m) \approx 0$, and C_T increases to 10^{-7}, which is typical for robust shock capturing with strong nonlinear adaptation. When $m \approx 0$, $g(m) \approx 1$ and $C_T \approx 10^{-10}$, which is suitable for resolving high-wavenumber physical fluctuations.

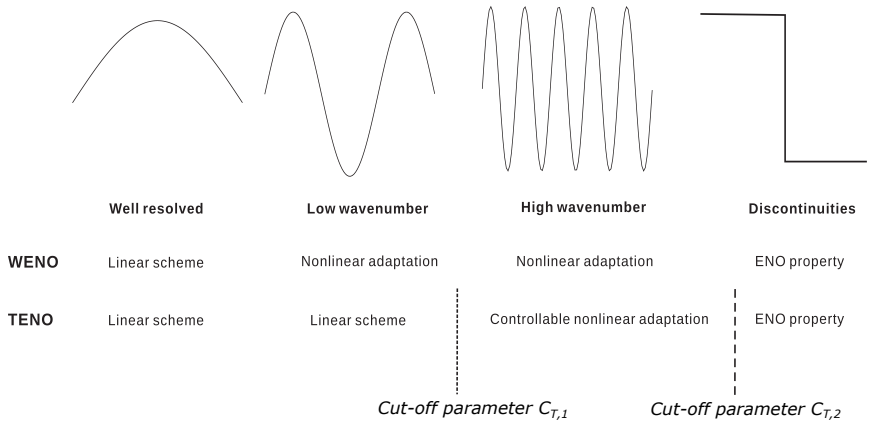

FIGURE 3. Resolution comparisons between WENO and TENO schemes (with adaptive dissipation control) for well-resolved scales, low-wavenumber scales, high-wavenumber scales and discontinuities.

Motivated by Ren & Zhang (2003), we employ

$$\begin{cases} m = 1 - \min(1, \eta_{i+1/2}/C_r), \\ \eta_{i+1/2} = \min(\eta_{i-1}, \eta_i, \eta_{i+1}, \eta_{i+2}), \end{cases} \tag{2.11}$$

where

$$\eta_i = \frac{\left|2\Delta f_{i+1/2}\Delta f_{i-1/2}\right| + \varepsilon}{\left(\Delta f_{i+1/2}\right)^2 + \left(\Delta f_{i-1/2}\right)^2 + \varepsilon}, \quad \text{with} \quad \varepsilon = \frac{0.9C_r}{1 - 0.9C_r}\xi^2. \tag{2.12}$$

The parameters are set as $\xi = 10^{-3}$ and $C_r = 0.27$.

The performance difference between the classical WENO scheme and the TENO scheme with adaptive dissipation control for resolving a wide range of scales is shown in Figure 3.

2.4. *High-order TENO-NA scheme*

Different from the original TENO schemes (Fu *et al.* 2016), the TENO weighting strategy is proposed to function as an explicit shock detector, which allows the design of a reconstruction scheme with optimal accuracy order even near the discontinuities (Fu *et al.* 2018*a*).

With the TENO weighting strategy, each candidate stencil is judged to be either smooth or non-smooth, i.e., crossing discontinuities. Considering the eight-point TENO scheme, as shown in Table 2.4, there are 17 combinations corresponding to 17 discontinuity distributions after discarding the unreasonable distributions by a voting strategy (Fu *et al.* 2018*a*). Based on the principle that the final reconstruction should not cross any discontinuity to enforce the ENO property, a target linear scheme optimized for highest accuracy order is adopted as the final reconstruction scheme according to each

combination, as given in

$$
\begin{aligned}
f_{i+1/2}^{opt,8} &= -0.007723831837710877 f_{i-3} + 0.05728582585522101 f_{i-2} \\
&-0.2148478198727312 f_{i-1} + 0.6852858258552214 f_i + 0.6152858258552207 f_{i+1} \\
&-0.1728478198727316 f_{i+2} + 0.04328582585522106 f_{i+3} - 0.005723831837710886 f_{i+4}.
\end{aligned} \tag{2.13}
$$

and

$$
\begin{aligned}
\hat{f}_{1,i+1/2} &= \frac{1}{420}(4f_{i-2} - 38f_{i-1} + 214f_i + 319f_{i+1} - 101f_{i+2} + 25f_{i+3} - 3f_{i+4}), \\
\hat{f}_{2,i+1/2} &= \frac{1}{60}(-2f_{i-1} + 22f_i + 57f_{i+1} - 23f_{i+2} + 7f_{i+3} - f_{i+4}), \\
\hat{f}_{3,i+1/2} &= \frac{1}{60}(12f_i + 77f_{i+1} - 43f_{i+2} + 17f_{i+3} - 3f_{i+4}), \\
\hat{f}_{4,i+1/2} &= \frac{1}{12}(-3f_{i-3} + 13f_{i-2} - 23f_{i-1} + 25f_i), \\
\hat{f}_{5,i+1/2} &= \frac{1}{60}(-3f_{i-3} + 17f_{i-2} - 43f_{i-1} + 77f_i + 12f_{i+1}), \\
\hat{f}_{6,i+1/2} &= \frac{1}{60}(-f_{i-3} + 7f_{i-2} - 23f_{i-1} + 57f_i + 22f_{i+1} - 2f_{i+2}), \\
\hat{f}_{7,i+1/2} &= \frac{1}{420}(-3f_{i-3} + 25f_{i-2} - 101f_{i-1} + 319f_i + 214f_{i+1} - 38f_{i+2} + 4f_{i+3}), \\
\hat{f}_{8,i+1/2} &= \frac{1}{60}(f_{i-2} - 8f_{i-1} + 37f_i + 37f_{i+1} - 8f_{i+2} + f_{i+3}), \\
\hat{f}_{9,i+1/2} &= \frac{1}{60}(2f_{i-2} - 13f_{i-1} + 47f_i + 27f_{i+1} - 3f_{i+2}), \\
\hat{f}_{10,i+1/2} &= \frac{1}{12}(-f_{i-1} + 7f_i + 7f_{i+1} - f_{i+2}), \\
\hat{f}_{11,i+1/2} &= \frac{1}{12}(f_{i-2} - 5f_{i-1} + 13f_i + 3f_{i+1}), \\
\hat{f}_{12,i+1/2} &= \frac{1}{60}(-3f_{i-1} + 27f_i + 47f_{i+1} - 13f_{i+2} + 2f_{i+3}), \\
\hat{f}_{13,i+1/2} &= \frac{1}{12}(3f_i + 13f_{i+1} - 5f_{i+2} + f_{i+3}), \\
\hat{f}_{14,i+1/2} &= \frac{1}{6}(-f_{i-1} + 5f_i + 2f_{i+1}), \\
\hat{f}_{15,i+1/2} &= \frac{1}{6}(2f_i + 5f_{i+1} - f_{i+2}), \\
\hat{f}_{16,i+1/2} &= \frac{1}{6}(2f_{i-2} - 7f_{i-1} + 11f_i).
\end{aligned} \tag{2.14}
$$

The eight-point TENO scheme with adaptive dissipation control is referred to as TENO8-NA.

3. Positivity-preserving TENO8-NA schemes

Based on the observation that the first-order Lax-Friedrichs flux

Reconstruction scheme	δ_0	δ_1	δ_2	δ_3	δ_4	δ_5
$\hat{f}^{opt,8}_{i+1/2}$	1	1	1	1	1	1
$\hat{f}_{1,i+1/2}$	1	1	1	1	0	1
$\hat{f}_{2,i+1/2}$	1	1	0	1	0	1
$\hat{f}_{3,i+1/2}$	0	1	0	1	0	1
$\hat{f}_{4,i+1/2}$	0	0	1	0	1	0
$\hat{f}_{5,i+1/2}$	1	0	1	0	1	0
$\hat{f}_{6,i+1/2}$	1	1	1	0	1	0
$\hat{f}_{7,i+1/2}$	1	1	1	1	1	0
$\hat{f}_{8,i+1/2}$	1	1	1	1	0	0
$\hat{f}_{9,i+1/2}$	1	1	1	0	0	0
$\hat{f}_{10,i+1/2}$	1	1	0	0	0	0
$\hat{f}_{11,i+1/2}$	1	0	1	0	0	0
$\hat{f}_{12,i+1/2}$	1	1	0	1	0	0
$\hat{f}_{13,i+1/2}$	0	1	0	1	0	0
$\hat{f}_{14,i+1/2}$	1	0	0	0	0	0
$\hat{f}_{15,i+1/2}$	0	1	0	0	0	0
$\hat{f}_{16,i+1/2}$	0	0	1	0	0	0

TABLE 1. Combinations of δ_k for the eight-point reconstruction schemes that avoid detected discontinuities.

$$\hat{\mathbf{F}}^{LF}_{i+1/2} = \frac{1}{2}[\mathbf{F}_i + \mathbf{F}_{i+1} + (|\mathbf{u}| + c)_{\max}(\mathbf{U}^n_i - \mathbf{U}^n_{i+1})] \tag{3.1}$$

has the positivity-preserving property under the CFL condition CFL $\leq 1/2$ (Perthame & Shu 1996), an *a posteriori*-based flux limiter has been proposed to recover the positivity of density and pressure by hybridizing the high-order flux and the first-order Lax-Friedrichs flux (Hu *et al.* 2013). Due to the convex property of the SSP Runge-Kutta method, the positivity-preserving limiter can be applied at each marching stage.

As shown in Zhang & Shu (2010) and Hu *et al.* (2013), with a careful design of the hybridizing strategy, the positivity-preserving limiter does not destroy the overall accuracy order and is activated locally for very few cells. Consequently, the dissipation and dispersion properties of the overall numerical method are determined mainly by the high-order shock-capturing scheme itself. The positivity-preserving limiter assures the nonlinear stability.

4. Numerical verification

In this section, two challenging benchmarks are simulated to validate the shock-capturing capability and the low-dissipation property of the present TENO8-NA scheme. For comparison, the results from the well-established classical WENO7-Z scheme will be presented. The parameters of the TENO8-NA scheme are fixed at the recommended values without case-by-case tuning.

The Roe method is applied for the characteristic decomposition of the Euler equations at the cell interface to avoid spurious oscillations. The 3rd-order SSP Runge-Kutta method is adopted for the time integral of the governing equations with a typical CFL

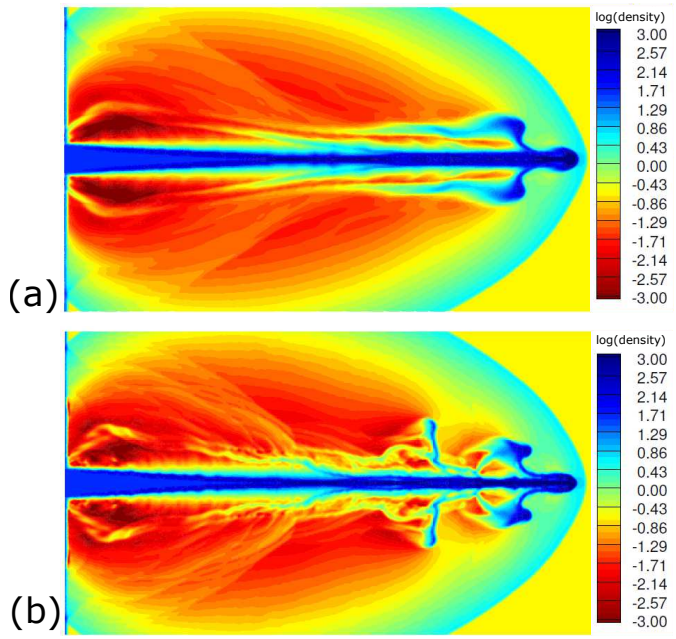

FIGURE 4. Logarithm of density distribution by WENO7-Z (a) and TENO8-NA (b) of a 2D high-Mach-number astrophysical jet with a Mach number of 80. The figures are drawn with 43 contour lines. The number of grid points is 448×224.

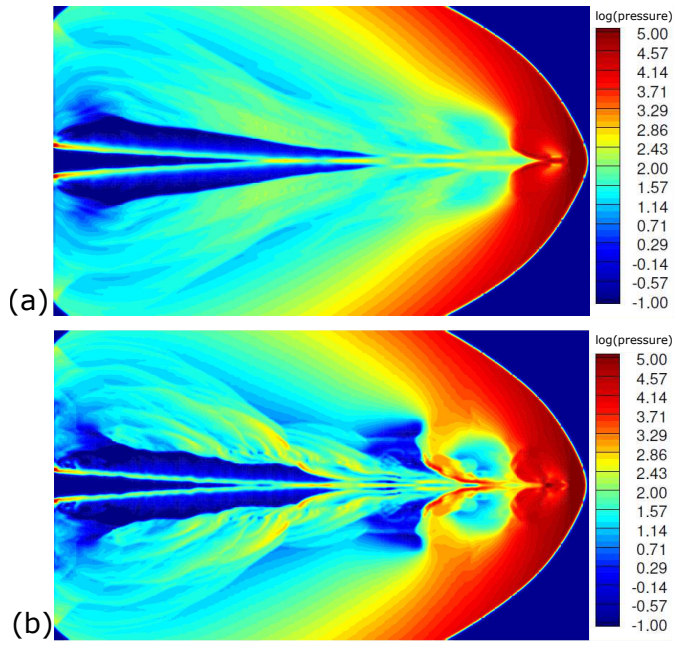

FIGURE 5. Logarithm of pressure distribution by WENO7-Z (a) and TENO8-NA (b) of a 2D high-Mach-number astrophysical jet with a Mach number of 80. The figures are drawn with 43 contour lines. The mesh number of grid points is 448×224.

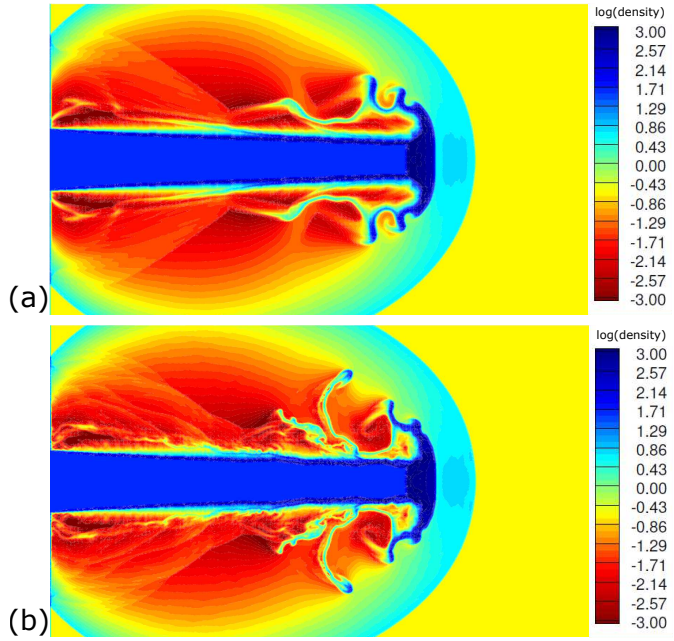

FIGURE 6. Logarithm of density distribution by WENO7-Z (a) and TENO8-NA (b) of a 2D high-Mach-number astrophysical jet with a Mach number of 2000. The figures are drawn with 43 contour lines. The number of grid points is 800×400.

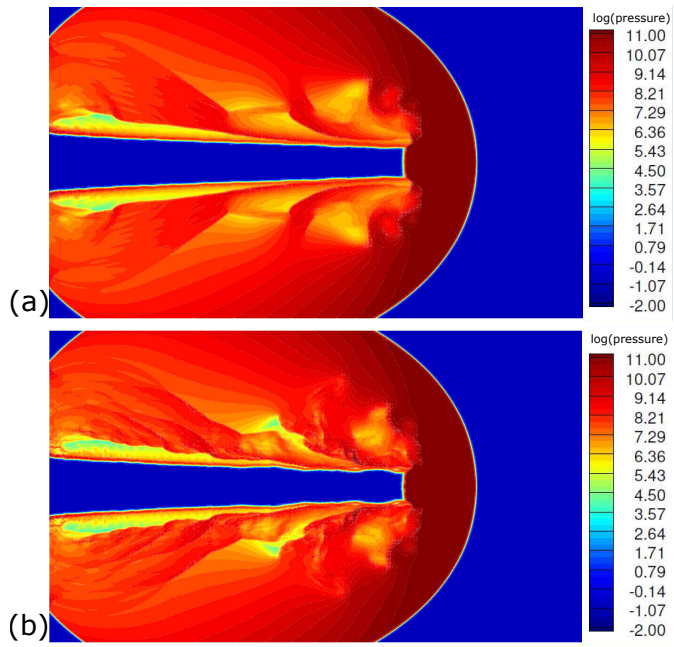

FIGURE 7. Logarithm of pressure distribution by WENO7-Z (a) and TENO8-NA (b) of a 2D high-Mach-number astrophysical jet with a Mach number of 2,000. The figures are drawn with 43 contour lines. The number of grid points is 800×400.

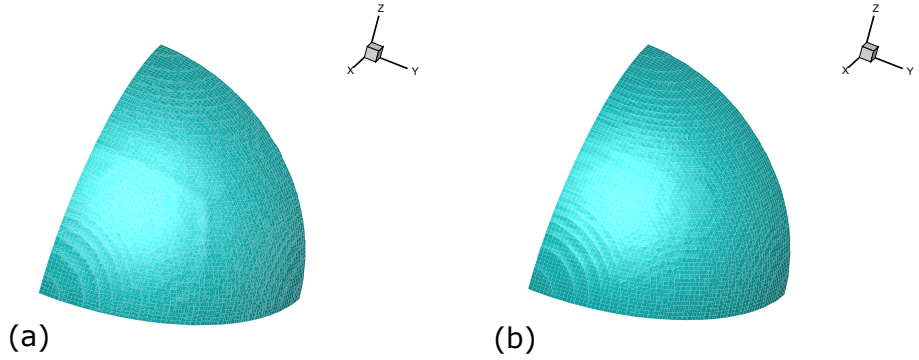

FIGURE 8. 3D Noh problem. Density iso-surface of $\rho = 50$ by WENO7-Z (a) and TENO8-NA (b). The mesh resolution is $64 \times 64 \times 64$.

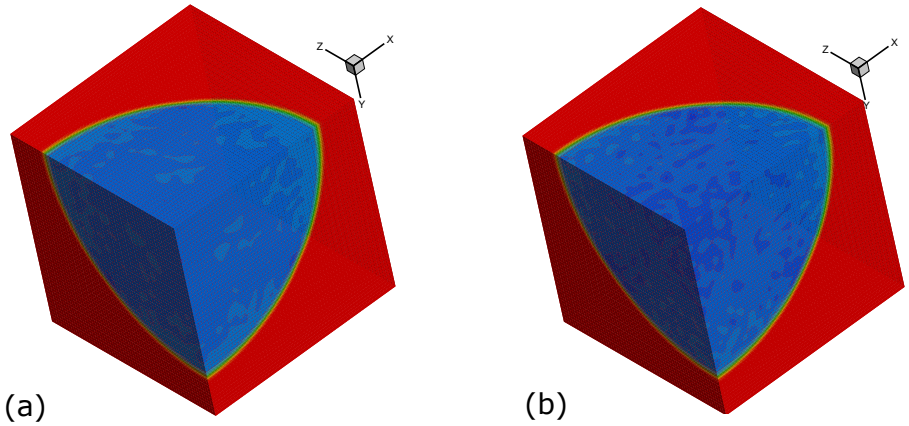

FIGURE 9. 3D Noh problem. Pressure distribution by WENO7-Z (a) and TENO8-NA (b). The pressure distribution is drawn with 43 contour lines between 0.5 and 23. The mesh resolution is $64 \times 64 \times 64$.

number of 0.4 unless otherwise mentioned. The positivity-preserving limiter is applied in a dimension-by-dimension manner.

4.1. *2D high-Mach-number astrophysical jet*

The simulations of two 2D high-Mach-number astrophysical jets without radiative cooling are considered (Zhang & Shu 2010). For the first case, the jet Mach number is 80, the computational domain is $x \in [0, 2]$ and $y \in [-0.5, 0.5]$ with ambient conditions of $(\rho, u, v, p) = (0.5, 0, 0, 0.4127)$. For the left boundary, $(\rho, u, v, p) = (5, 30, 0, 0.4127)$ if $y \in [-0.05, 0.05]$ and $(\rho, u, v, p) = (5, 0, 0, 0.4127)$ otherwise. For the second case, the jet Mach number is 2000 and the computational domain is $x \in [0, 1]$ and $y \in [-0.25, 0.25]$. The boundary conditions are the same as for the first case except on the left boundary, $u = 800$ if $y \in [-0.05, 0.05]$. For both cases, the right, top and bottom boundaries are non-reflecting outflows and the ratio of specific heats is $\gamma = 5/3$. The number of grid points for each case is 448×224 and 800×400, respectively.

As shown in Figures 4–7, the TENO8-NA scheme resolves significantly more small-scale

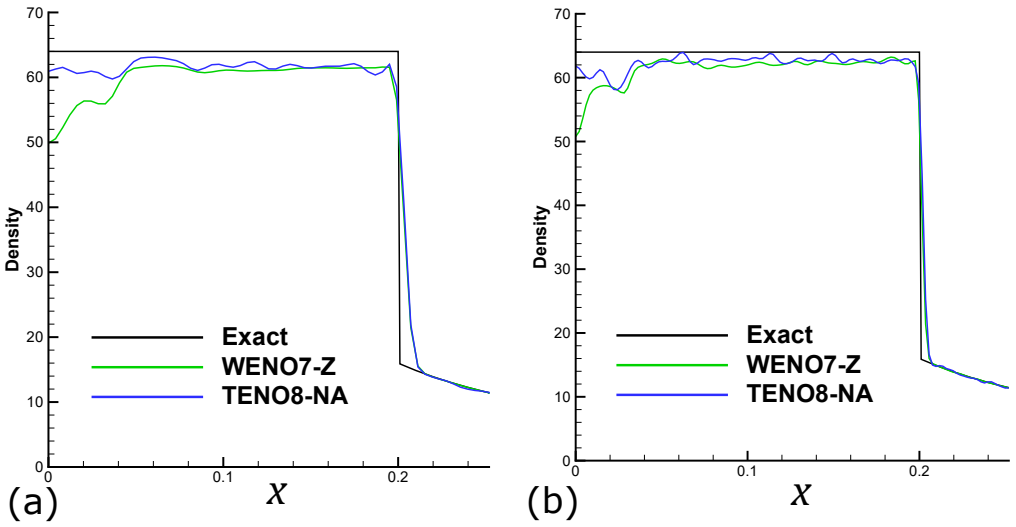

FIGURE 10. 3D Noh problem. Density profiles from TENO8-NA and WENO7-Z. The mesh resolutions are $64 \times 64 \times 64$ (a) and $128 \times 128 \times 128$ (b).

structures than the classical WENO7-Z scheme does. Note that, the strong shock fronts for both Mach numbers are captured by the WENO7-Z and the TENO8-NA schemes without carbuncle problems, which typically occur for multidimensional shock-capturing methods (Robinet *et al.* 2000).

4.2. *3D Noh problem*

We consider the Noh problem (Noh 1987), where the uniform implosion of an ideal gas leads to a shock of infinite strength and thus greatly challenges the numerical algorithms. The computational domain is $[0, 0.256] \times [0, 0.256] \times [0, 0.256]$ and the ratio of specific heats is $\gamma = 5/3$. The initial condition is given as $(\rho, u, v, p) = (1, -x/r, -y/r, 10^{-6})$, where $r = \sqrt{x_i x_i}$ and the small value of 10^{-6} is adopted to prevent complex eigenvalues (Kawai *et al.* 2010). Symmetry conditions are imposed along $x_i = 0$ while supersonic inflows are imposed on the remaining boundaries with the velocity and pressure from the initial condition and the density from the analytical solution. For the spherical geometry, the shock wave moves radially outward with a constant speed of 1/3. The analytical solution for the density in three dimensions is

$$\rho = \begin{cases} 64, & r < t/3, \\ (1 + t/r)^2, & r \geq t/3. \end{cases} \tag{4.1}$$

In this case, the global Lax-Friedrichs scheme (Jiang & Shu 1996) is adopted for flux splitting. The mesh resolutions are $64 \times 64 \times 64$ and $128 \times 128 \times 128$.

As shown in Figure 8, the result from the WENO7-Z scheme has a slight grid-alignment artifact, which is not observed for the TENO8-NA scheme. This artifact shows up as a slight wrinkle in the nearly spherical shell along its intersection with the plane $x/x_{max} \approx 0.5$ and the intersection of the spherical shell with the plane $y/y_{max} \approx 0.5$. Figure 9 shows the pressure distributions; both schemes are free from the shock-induced instabilities.

As shown in Figure 10, the agreement of the computed density distribution with the analytical solution is better for TENO8-NA than for WENO7-Z. In particular, the over-

heating problem at the origin, which is observed for most numerical methods (see Figure 10 of Johnsen *et al.* 2010), is greatly improved by TENO8-NA at both resolutions.

5. Conclusions

In this paper, we have investigated the performance of high-order TENO schemes for two extreme simulations. Numerical experiments demonstrate that, in combination with a positivity-preserving limiter, which does not destroy the accuracy order, the presented TENO scheme can handle very-high-Mach-number flows with low numerical dissipation and sharp shock-capturing capability. Future work will focus on extending the present scheme to more complex geometries and more complex physics, e.g., multiphase flows, magneto-hydrodynamics, and combustion.

Acknowledgments

This work was supported by NASA's Transformational Tools and Technologies project under grant number NNX15AU93A. K.G. acknowledges support from the NDSEG and Stanford Graduate Fellowships.

REFERENCES

Adams, N. & Shariff, K. 1996 A high-resolution hybrid compact-ENO scheme for shock-turbulence interaction problems. *J. Comput. Phys.* **127**, 27–51.

Borges, R., Carmona, M., Costa, B. & Don, W. S. 2008 An improved weighted essentially non-oscillatory scheme for hyperbolic conservation laws. *J. Comput. Phys.* **227**, 3191–3211.

Di Renzo, M., Fu, L. & Urzay, J. 2020 HTR solver: An open-source exascale-oriented task-based multi-GPU high-order code for hypersonic aerothermodynamics. *Comput. Phys. Commun.* **255**, 107262.

Di Renzo, M. & Urzay, J. 2021 Direct numerical simulation of a hypersonic transitional boundary layer at suborbital enthalpies. *J. Fluid Mech.* **912**, A29.

Dong, H., Fu, L., Zhang, F., Liu, Y. & Liu, J. 2019 Detonation simulations with a fifth-order TENO scheme. *Commun. Comput. Phys.* **25**, 1357–1393.

Fu, L. 2018 A low-dissipation finite-volume method based on a new TENO shock-capturing scheme. *Comput. Phys. Commun.* **235**, 25–39.

Fu, L., Hu, X. Y. & Adams, N. A. 2016 A family of high-order targeted ENO schemes for compressible-fluid simulations. *J. Comput. Phys.* **305**, 333–359.

Fu, L., Hu, X. Y. & Adams, N. A. 2017 Targeted ENO schemes with tailored resolution property for hyperbolic conservation laws. *J. Comput. Phys.* **349**, 97–121.

Fu, L., Hu, X. Y. & Adams, N. A. 2018*a* A new class of adaptive high-order targeted ENO schemes for hyperbolic conservation laws. *J. Comput. Phys.* **374**, 724–751.

Fu, L., Hu, X. Y. & Adams, N. A. 2018*b* A targeted ENO scheme as implicit model for turbulent and genuine subgrid scales. *Commun. Comput. Phys.* **26**, 311–345.

Fu, L., Karp, M., Bose, S. T., Moin, P., & Urzay, J. 2021 Shock-induced heating and transition to turbulence in a hypersonic boundary layer. *J. Fluid Mech.* **909**, A8.

Gerolymos, G., Sénéchal, D. & Vallet, I. 2009 Very-high-order WENO schemes. *J. Comput. Phys.* **228**, 8481–8524.

Griffin, K. P., Fu, L., & Moin, P. 2021 Velocity transformation for compressible wall-bounded turbulent flows with and without heat transfer. *P. Natl. Acad. Sci. USA.* **118**, e2111144118.

Haimovich, O. & Frankel, S. H. 2017 Numerical simulations of compressible multicomponent and multiphase flow using a high-order targeted ENO (TENO) finite-volume method. *Comput. Fluids* **146**, 105–116.

Harten, A. 1983 A high resolution scheme for the computation of weak solutions of hyperbolic conservation laws. *J. Comput. Phys.* **49**, 357–393.

Harten, A., Engquist, B., Osher, S. & Chakravarthy, S. R. 1987 Uniformly high order accurate essentially non-oscillatory schemes, III. *J. Comput. Phys.* **71**, 231–303.

Henrick, A. K., Aslam, T. & Powers, J. M. 2005 Mapped weighted essentially non-oscillatory schemes: achieving optimal order near critical points. *J. Comput. Phys.* **207**, 542–567.

Hu, X. Y., Adams, N. A. & Shu, C.-W. 2013 Positivity-preserving method for high-order conservative schemes solving compressible Euler equations. *J. Comput. Phys.* **242**, 169–180.

Jameson, A. 1994 Analysis and design of numerical schemes for gas dynamics, 1: artificial diffusion, upwind biasing, limiters and their effect on accuracy and multigrid convergence. *Int. J. Comput. Fluid D.* **4**, 171–218.

Jiang, G. S. & Shu, C.-W. 1996 Efficient implementation of weighted ENO schemes. *J. Comput. Phys.* **126**, 202–228.

Johnsen, E., Larsson, J., Bhagatwala, A. V., Cabot, W. H., *et al.* 2010 Assessment of high-resolution methods for numerical simulations of compressible turbulence with shock waves. *J. Comput. Phys.* **229**, 1213–1237.

Kawai, S., Shankar, S. K. & Lele, S. K. 2010 Assessment of localized artificial diffusivity scheme for large-eddy simulation of compressible turbulent flows. *J. Comput. Phys.* **229**, 1739–1762.

Lele, S. K. 1992 Compact finite difference schemes with spectral-like resolution. *J. Comput. Phys.* **103**, 16–42.

Liu, X. D., Osher, S. & Chan, T. 1994 Weighted essentially non-oscillatory schemes. *J. Comput. Phys.* **115**, 200–212.

Noh, W. F. 1987 Errors for calculations of strong shocks using an artificial viscosity and an artificial heat flux. *J. Comput. Phys.* **72**, 78–120.

Perthame, B. & Shu, C.-W. 1996 On positivity preserving finite volume schemes for Euler equations. *Numer. Math.* **73**, 119–130.

Pirozzoli, S. 2011 Numerical methods for high-speed flows. *Annu. Rev. Fluid Mech.* **42**, 163–194.

Ren, Y.-X. & Zhang, H. 2003 A characteristic-wise hybrid compact-WENO scheme for solving hyperbolic conservation laws. *J. Comput. Phys.* **192**, 365–386.

Robinet, J.-C., Gressier, J., Casalis, G. & Moschetta, J.-M. 2000 Shock wave instability and the carbuncle phenomenon: same intrinsic origin? *J. Fluid Mech.* **417**, 237–263.

Shu, C.-W. 2009 High order weighted essentially nonoscillatory schemes for convection dominated problems. *SIAM Rev.* **51**, 82–126.

Sun, Z., Inaba, S. & Xiao, F. 2016 Boundary variation diminishing (bvd) reconstruction: A new approach to improve Godunov schemes. *J. Comput. Phys.* **322**, 309–325.

Suresh, A. & Huynhb, H. 1997 Accurate monotonicity-preserving schemes with Runge-Kutta time stepping. *J. Comput. Phys.* **136**, 83–99.

Titarev, V. & Toro, E. 2004 Finite-volume WENO schemes for three-dimensional conservation laws. *J. Comput. Phys.* **201**, 238–260.

Urzay, J. 2018 Supersonic combustion in air-breathing propulsion systems for hypersonic flight. *Annu. Rev. Fluid Mech.* **50**, 593–627.

Von, N. J. & Richtmyer, R. 1950 A method for the numerical calculation of hydrodynamic shocks. *J. Appl. Phys.* **21**, 232.

Weirs, V. & Candler, G. 1997 Optimization of weighted ENO schemes for DNS of compressible turbulence. *13th Computational Fluid Dynamics Conference,* p. 1940.

Zhang, X. & Shu, C.-W. 2010 On positivity-preserving high order discontinuous Galerkin schemes for compressible Euler equations on rectangular meshes. *J. Comput. Phys.* **229**, 8918–8934.

Zhang, X. & Shu, C.-W. 2012 Positivity-preserving high order finite difference WENO schemes for compressible Euler equations. *J. Comput. Phys.* **231**, 2245–2258.